Biochimica et Biophysica Acta 1838 (2014) 2852–2860

Contents lists available at ScienceDirect

Biochimica et Biophysica Acta

journal homepage: www.elsevier.com/locate/bbamem

Atomistic simulations of anionic $Au_{144}(SR)_{60}$ nanoparticles interacting with asymmetric model lipid membranes

Elena Heikkilä [a,b,1,2], Hector Martinez-Seara [a,1], Andrey A. Gurtovenko [c,d,3,4], Ilpo Vattulainen [a,e,1,5], Jaakko Akola [a,b,f,*,1,2,6]

[a] Department of Physics, Tampere University of Technology, P.O. Box 692, FI-33101 Tampere, Finland
[b] COMP Centre of Excellence, Department of Applied Physics, Aalto University, FI-00076, AALTO, Finland
[c] Institute of Macromolecular Compounds, Russian Academy of Sciences, Bolshoi Prospect 31, V.O., St. Petersburg 199004, Russia
[d] Department of Molecular Biophysics, Faculty of Physics, St. Petersburg State University, St. Petersburg 198504, Russia
[e] Center for Biomembrane Physics (MEMPHYS), University of Southern Denmark, Odense DK-5230, Denmark
[f] PGI-1, Forschungszentrum Jülich, D-52425 Jülich, Germany

ARTICLE INFO

Article history:
Received 9 May 2014
Received in revised form 17 July 2014
Accepted 31 July 2014
Available online 7 August 2014

Keywords:
Gold nanoparticle
Anionic nanoparticle
Lipid bilayer
Plasma membrane
Molecular dynamics
Atomistic simulations

ABSTRACT

Experimental observations indicate that the interaction between nanoparticles and lipid membranes varies according to the nanoparticle charge and the chemical nature of their protecting side groups. We report atomistic simulations of an anionic Au nanoparticle ($AuNP^-$) interacting with membranes whose lipid composition and transmembrane distribution are to a large extent consistent with real plasma membranes of eukaryotic cells. To this end, we use a model system which comprises two cellular compartments, extracellular and cytosolic, divided by two asymmetric lipid bilayers. The simulations clearly show that $AuNP^-$ attaches to the extracellular membrane surface within a few tens of nanoseconds, while it avoids contact with the membrane on the cytosolic side. This behavior stems from several factors. In essence, when the nanoparticle interacts with lipids in the extracellular compartment, it forms relatively weak contacts with the zwitterionic head groups (in particular choline) of the phosphatidylcholine lipids. Consequently, $AuNP^-$ does not immerse deeply in the leaflet, enabling, *e.g.*, lateral diffusion of the nanoparticle along the surface. On the cytosolic side, $AuNP^-$ remains in the water phase due to Coulomb repulsion that arises from negatively charged phosphatidylserine lipids interacting with $AuNP^-$. A number of structural and dynamical features resulting from these basic phenomena are discussed. We close the article with a brief discussion of potential implications.

1. Introduction

Gold nanoparticles (AuNPs) are useful in medical applications, such as in targeted drug delivery, drug release, and photo-thermal therapy [1,2]. However, nanoscale gold can also cause harmful side effects for living organisms that induce cell death [3,4]. In particular, cationic nanoparticles of 2 nm diameter or less have an enhanced cytotoxic activity [5–9], as demonstrated for 1.4 nm AuNPs, which were observed to cause necrosis and mitochondrial damage to various cell lines [10]. Experimental results suggest self-penetration as the potential membrane translocation mechanism. The process is affected by the AuNP charge and the composition of the protecting ligand shell. Cationic AuNPs with an alternating pattern of aliphatic (hydrophobic) and functionalized side groups, the so-called striped AuNPs, show increased penetration activity in comparison to randomly distributed functionalized side groups [11]. Therefore, it can be also concluded that the role of the gold core itself is less important for the translocation process due to the crowding of surrounding surfactants. The penetration activity of cationic AuNPs has been reported to generate holes in model and living membranes, where the level of disruption depends on the initial phase of the lipid bilayer [5,12–14].

Anionic gold nanoparticles appear to have less effect on membranes. However, also anionic nanoparticles have been shown to interact with cells, and it is of importance to shed light on the details of these interactions on cellular level. Furthermore, understanding what makes anionic nanoparticles less active on cells can promote the development of safer and less toxic nanoparticle applications. Recently, it was demonstrated that anionic striped AuNPs, which comprise an amphiphilic surface, can permeate non-disruptively through model membranes with size-dependent activity [15]. Furthermore, the nanoparticle-membrane interaction has been studied for 2 nm diameter AuNPs and model

* Corresponding author at: Department of Physics, Tampere University of Technology, P.O. Box 692, FI-33101 Tampere, Finland.
E-mail address: jaakko.akola@tut.fi (J. Akola).
[1] Tampere University of Technology.
[2] Aalto University.
[3] Russian Academy of Sciences.
[4] St. Petersburg State University.
[5] University of Southern Denmark.
[6] Forschungszentrum Jülich.

http://dx.doi.org/10.1016/j.bbamem.2014.07.027
0005-2736/

membranes by Tatur *et al.* [16] by following the activity of floating AuNPs between single-component bilayers comprised of zwitterionic DSPC lipids (1,2-distearoyl-*sn*-glycero-3-phosphocholine). The neutron reflectometry measurements indicated that AuNPs with cationic terminal groups penetrate inside the hydrophobic bilayer interior (after elevating the temperature up to 53 °C) and result in membrane disruption at increased concentrations. There was no such effect observed for anionic AuNPs, which stayed outside the lipid bilayers. The results by Tatur *et al.* for model membranes provide a valuable reference for simulations enabling a direct comparison between theory and experiments as there are no complicating factors arising from other components in real membranes (*e.g.*, membrane proteins and glycocalyx networks).

The effects of AuNPs on cell membranes and their nanotoxicity needs to be investigated in order to estimate potential risks in various biomedical and nanotechnological applications. Here, atomistic level simulations are able to provide new detailed information on the AuNP-membrane interaction. We have previously studied the interaction of a cationic AuNP with asymmetric lipid membranes, and our results showed that the cationic nanoparticle attaches to the bilayer surface on both the extracellular (EC) and intracellular (IC) sides [17]. However, the simulation results showed that the membrane leaflet binding to the cationic AuNP adjusts to the presence of the nanoparticle differently. On the EC side there is a rearrangement of zwitterionic lipids and nanoparticle side groups in the contact area, giving rise to the initial stage of pore formation on the membrane surface. This behavior is not observed on the IC side, where the cationic AuNP is spontaneously captured by the negatively charged phosphatidylserine lipids that diffuse underneath the nanoparticle.

In this work, we have performed a series of atomistic molecular dynamics (MD) simulations for an anionic monolayer-protected AuNP with functionalized (charged) alkanethiol side groups [$Au_{144}(SR)_{60}$ where $R = C_{11}H_{22}$ + carboxylic group] in aqueous solution in the presence of asymmetric lipid bilayers by using a double membrane setup [17] which divides the system into two compartments, EC and IC, depending on the leaflet next to the nanoparticle and the counterion composition. The lipid composition was chosen to be representative of an animal plasma membrane (the POPS fraction in membrane leaflets of mammalian cells is most commonly in the range of 10–20% 28–30), and it comprises zwitterionic POPC [1-palmitoyl-2-oleoyl-*sn*-glycero-3-phosphocholine] in the outer EC leaflet, while a mixture of POPC (81.25 mol%) and negatively charged POPS [1-palmitoyl-2-oleoyl-*sn*-glycero-3-phosphoserine] (18.75 mol%) is used for the inner IC leaflet.

The present study is a continuation of our previous work, where we considered, among other topics, anionic AuNPs in aqueous solution (in the absence of lipid membranes) [18]. Here, $AuNP^-$ was simulated over an extensive period of 200 ns in double membrane systems, both in the EC and IC compartments, with and without salt. The purpose was to mimic the EC and IC fluids by adding a biologically relevant concentration of salt (150 mM) into the compartments. Simulations were performed both with counterions only and with counterions and salt to monitor the effects of the added salt on the systems. Furthermore, performing simulations/analysis of systems also without added salt made comparisons to our previous study of AuNPs in aqueous solution [18] more straightforward. As control set-ups, the corresponding reference configurations of the double membrane systems without the nanoparticle were also simulated. Our simulations complement previous theoretical work on AuNPs interacting with lipid bilayers [19–24] [coarse-grained models (CG)] and AuNPs with solvent-effects (atomistic simulations), [25,26] and provide new insights to $AuNP^-$ membrane interactions at the atomistic level.

Here, we observe that $AuNP^-$ attaches to the EC leaflet despite the fact that the overall charge of the membrane is negative. The nanoparticle-membrane interaction is mediated by the contact between terminal carboxylate ($AuNP^-$) and positively charged POPC choline groups, but it is rather weak and does not lead to nanoparticle immersion to the membrane. Consequently, $AuNP^-$ floats on top of the EC leaflet, allowing it to diffuse laterally along the membrane plane. The nanoparticle does not desorb spontaneously back to the water phase, indicating that there is quite a deep free energy barrier at the membrane-water interface region, and by residing therein, $AuNP^-$ alters some of the structural and dynamical properties of the membrane (see Section 3). On the IC side, $AuNP^-$ does not bind to the membrane due to repulsive interaction with the negatively charged POPS lipids, thus also structural perturbations are limited. We close the article with a brief discussion of potential implications.

2. Materials and methods

The monolayer-protected gold nanoparticle (AuNP) of 144 Au atoms has been modeled with functionalized alkanethiol tail groups (undecanyl chain, $R = C_{11}H_{22}$, and a carboxylate terminal group), as described more in detail elsewhere [18]. The alkanethiol chains are modeled based on the united atom concept [27] that describes a CH_2 group as a single "united" bead. This approach includes explicit representation of polar hydrogen atoms, while nonpolar hydrogens are being excluded. The rigid 114-atom gold core possesses a nearly-spherical polyhedral geometry (rhombicosidodecahedron) based on the previous theoretical suggestion that fitted experimental X-ray data (structure factor) and was consistent with voltammetric measurements for different charge states of the metallic core [28]. The monolayer covering the Au core consists of 30 "oxidized" surface Au atoms and 60 alkylthiol ligands ($SR-$ with $R = C_{11}H_{22}$) with polar tail groups, and two ligands attached to each surface gold atom [18]. Each hydrocarbon chain is terminated by a terminal carboxylate group COO^- making the nanoparticle strongly charged, and the molecular formula of the particle can be represented as $Au_{144}(SRCOO-)_{60}$.

Gold nanoparticles are charged, and one has to treat the electrostatics of the membrane as accurately as possible. Here, it is important to realize that in addition to zwitterionic lipids, the plasma membranes contain a certain amount of charged (anionic) lipids which are essential for the AuNP-membrane interactions [17]. Furthermore, the anionic lipids such as POPS are localized mostly within the inner leaflets of plasma membranes. To address all these issues, we inserted anionic POPS lipids in one of the POPC leaflets. The leaflets were taken from the corresponding symmetric POPC bilayer, and special care was paid to build a tensionless membrane. The POPS fraction in membrane leaflets of mammalian cells varies rather widely depending on the cell type, but normally does not exceed 0.3, most commonly being in the range of 0.1–0.2 [29–31]. Therefore, a valid fraction close to 0.2 was chosen for simulations. A symmetric POPC/POPS membrane was then built as follows: 24 head groups of PC lipids randomly chosen in each leaflet of the POPC membrane were converted to PS head groups. The resulting symmetric PC/PS lipid membrane was equilibrated for 20 ns. To match the areas of symmetric POPC and POPC/POPS membranes, 8 lipids were removed from the original POPC membrane, giving rise to a bilayer of 248 POPC lipids. The resulting asymmetric POPC/POPS lipid membrane was equilibrated for 10 ns before it was used to build up a double bilayer system. This procedure allows us to explicitly take into account the asymmetric transmembrane distribution of anionic lipids inherent for plasma membranes of eukaryotic cells, keeping the membrane model relatively simple. Further developments could involve including other essential lipid components into the membrane model, such as sphingomyelin, phosphatidyl-ethanolamine, and cholesterol, but those remain to be considered in future studies.

The simulation setup of $AuNP^-$ and two asymmetric lipid bilayers is visualized for three different cases in Fig. 1. The simulation box dimensions were adjusted to $9 \times 9 \times 22$ nm for the nanoparticle-membrane simulations with a double membrane setup. The asymmetric lipid bilayers were comprised of two different membrane leaflets, where the cytosolic (IC) leaflet consisted of a mixture of 104 POPC and 24 POPS lipids and the EC leaflet was comprised of 124 POPCs. Based on tests, this choice of lipid numbers was confirmed to result in flat lipid bilayers

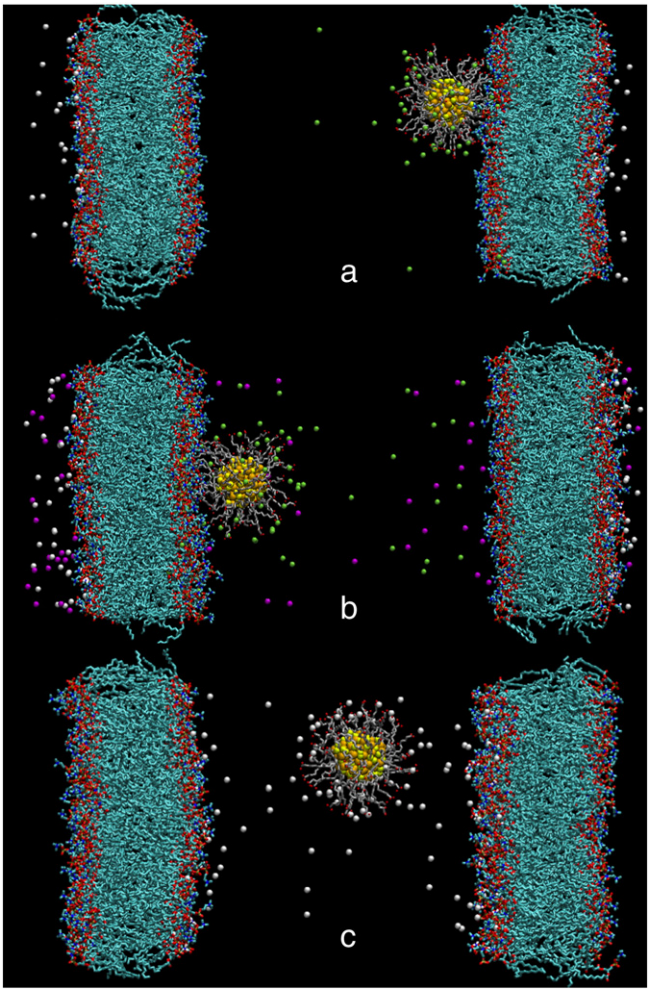

Fig. 1. Visualization of $AuNP^-$ with membranes. $AuNP^-$ is placed between two lipid bilayers in extracellular (EC) and intracellular (IC) compartments. (a) EC, (b) EC with salt, and (c) IC. The snapshots were taken from the middle of the 200-ns trajectories; the position of $AuNP^-$ with respect to the membranes is spontaneous in all figures. After an initial equilibration, $AuNP^-$ fluctuates close to these positions during the rest of the simulations. Color code: Au (gold), S (yellow), C (gray, CPK), O (red), N (blue), P (maroon), Na^+ (lime), Cl^- (magenta), K^+ (white), and lipid bilayer carbons (cyan).

(with no spontaneous curvature). Two of such asymmetric lipid bilayers were inserted into the simulation box such that the IC leaflets of the bilayers were face-to-face (membrane inversion). After placing $AuNP^-$ into the simulation box, it was filled with water, and 60 Na^+ (EC compartment) or 60 K^+ (IC compartment) counterions were added to the system, and additional 24 K^+ ions were put in to compensate for POPS charges on the IC side. In one case, we also added 150 mM of salt to the water phases (Na^+Cl^- to the EC compartment, K^+Cl^- to the IC compartment). The aim was to mimic cytosolic and extracellular fluids in mammalian cells by using K^+ and Na^+ ions, inside and outside the cell, respectively. The bilayer center of masses (COMs) were separated by a distance of (15.1 ± 0.2) nm across the compartment containing $AuNP^-$, which is significantly larger than the bilayer thickness of (3.8 ± 0.1 nm, P–P distance across the leaflets) and the nanoparticle diameter of about 4.1 nm [18]. The chosen system sizes were confirmed to be consistent with the water density at the given temperature (T = 310 K) to set up a realistic simulation system with an appropriate amount of water. The overall number of atoms in the simulated $AuNP^-$ systems was around 143,000.

The simulations were carried out using a united atom force field which is largely compatible with the Berger force field [32], and it is a mixture of a tuned united OPLS (non-bonded interactions) and GROMOS (bonded interactions) force fields. The POPC lipids are implemented as originally developed by Berger *et al.* [33,33] with adjustments for the double bond [34]. The POPS force field model follows the Mukhopadhyay *et al.* implementation [35]. The $AuNP^-$ composition and force field have been described in Heikkilä *et al.* [18], and water molecules were represented using the SPC model [36]. The counterions Na^+, Cl^-, and K^+ use their original GROMACS-87 parameters [37]. The particle-mesh Ewald summation (PME) method [38] was used for electrostatic interactions with a real space cut-off of 1.0 nm and a reciprocal grid of 77 × 78 × 189 cells with a 4th order *B*-spline interpolation. For van der Waals interactions, we used a cut-off distance of 1.0 nm.

The MD simulations were performed by using the GROMACS program package [39] (versions 4.0.5 and 4.5.6) in the canonical *NPT* ensemble by setting the temperature to 310 K using the Berendsen thermostat [40] with a time constant of 0.1 ps. The coupled barostat applied a semi-isotropic pressure coupling using the Berendsen algorithm [40] with compressibility of $4.5 \times 10^{-5} \cdot bar^{-1}$, time constant of 5 ps and reference pressure of 1 bar. The time step was set to 2 fs and the neighbor list (cut-off 1.0 nm) was updated for every 10th frame (20 fs). The SHAKE algorithm [41] was employed in the simulations. The prepared systems were energy minimized and each system was allowed to equilibrate for 50 ns at the target temperature before the actual production simulation was started.

The dynamics of $AuNP^-$ was simulated in the EC and IC compartments of the double membrane system, and the details of these simulations are summarized in Table 1. First, $AuNP^-$ with counterions was simulated in the EC and IC sides for 200 ns (2 × 200 ns storing data every 10 ps). Additional simulations were carried out four times with the same parameters and coordinates but with different initial velocities, each for 100 ns (2 × 4 × 100 ns) in order to gain more statistics. In addition to $AuNP^-$/counterion simulations, 150 mM of salt was added in both compartments and MD simulations were performed for 200 ns. In order to study particularly rapid processes related to water hydrogen bonds (H-bonds) and counterion contacts between $AuNP^-$ and the surrounding solution, ten shorter simulations with a more frequent data storage rate $(0.5\ ps)^{-1}$ were run (10 × 1 ns) starting from different snapshots of the longest 200 ns simulation trajectory for each system. Snapshots were taken from the time window between 100 and 200 ns, and they were separated by 10 ns. The purpose was to use uncorrelated starting structures for the 1-ns simulations.

As a reference, a 200-ns simulation without $AuNP^-$ was performed for the double bilayer systems, where the simulation box dimensions were adjusted to 9 × 9 × 13 nm. Both compartments were filled with water and 48 K^+ ions to the IC side to compensate for the negative charge of POPS lipids. In the reference simulation the bilayers were (3.6 ± 0.1) nm thick and separated by a distance of (7.0 ± 0.2) nm, as determined based on the average P–P distances of the corresponding leaflet pairs.

To visualize the ionic cloud around the nanoparticle in the presence of a membrane, 60-ns simulations were performed (both in EC and IC) constraining the distance between the center of masses of the Au core and POPC lipid P atoms of the closest leaflet to 2.84 nm by using a force constant of 10,000 $kJ \cdot mol^{-1} \cdot nm^{-1}$. The visualization was carried out using VMD [42]. The VolMap tool of the VMD plugin library was used for ion density calculation with a resolution of 0.5 Å and using an atom size parameter of 1.0, averaging over all frames of the 60-ns trajectory.

The structure of the membrane in the presence or absence of $AuNP^-$ was studied by calculating order parameters for POPC lipid hydrocarbon chains. The order parameters were computed using the angle θ between the bilayer surface normal and a vector between two lipid carbon palmitoyl tail atoms, C_{n-1} and C_{n+1}:[43, 44]

$$S_{CD} = \frac{3}{2}\ \cos^2\theta\ - \frac{1}{2}. \quad (1)$$

In cases where the $AuNP^-$ approached the bilayer (EC), the order parameter was also calculated separately for lipids that were right in

Table 1
Simulations of $AuNP^-$ membrane systems. Charges compensating counterions were used in the solvent for each system with $AuNP^-$, and all systems contained counterions for POPS lipids. In one case, salt (150 mM) was added into both compartments. The "constr." cases refer to simulations with constrained nanoparticle-membrane distance of 2.8 nm. The reference system is a double membrane system without $AuNP^-$. The columns for the EC and IC compartments show the constituents, in addition to water.

Setup	EC compartment	IC compartment	Simulations
$AuNP^-$@EC	$AuNP^-$, Na^+	K^+	1 × 200 ns, 4 × 100 ns, 10 × 1 ns
$AuNP^-$@EC + salt	$AuNP^-$, Na^+, Na^+ Cl^-	K^+, K^+ Cl^-	1 × 200 ns, 10 × 1 ns
$AuNP^-$@EC constr.	$AuNP^-$, Na^+	K^+	1 × 60 ns
$AuNP^-$@IC	–	$AuNP^-$, K^+	1 × 200 ns, 4 × 100 ns, 10 × 1 ns
$AuNP^-$@IC constr.	–	$AuNP^-$, K^+	1 × 60 ns
Reference	–	K^+	1 × 200 ns, 10 × 1 ns

the vicinity of $AuNP^-$: To this end, we considered only those lipids whose nitrogen atom (choline) in the lipid head group was closer than a cut-off distance (3 nm) from the nanoparticle COM. The error of the order parameter was estimated to be no more than ± 0.001 due to extensive sampling.

The analysis of H-bonds and ionic contacts was carried out by averaging over the time windows with a more frequent data storage rate of ($\Delta t = 0.5$ ps). Contacts between the $AuNP^-$ terminal groups, water molecules, and membrane head groups were considered within a cut-off distance of 0.35 nm for non-hydrogen atoms and an H-bond angle of 30°. Similarly, a cut-off distance of 0.35 nm was used for ionic bonds/contacts.

To characterize the diffusive motion of water and ions around $AuNP^-$, we computed their short-time diffusion factor M inside slices of thickness $\Delta r = 0.5$ nm (water) and 1.0 nm (counterions) between the two membranes along the membrane surface normal. For every time step n ($t = n\Delta t$) during the simulation, we determined the water molecules and ions that were at a given distance within the compartment, after which we determined the mean-square displacement $\mathrm{MSD}_A(t)$ of particles of type A (ions, water, *etc.*) as follows:

$$\mathrm{MSD}_A(t) = \left\langle |\mathrm{r}_i(t) - \mathrm{r}_i(0)|^2 \right\rangle_{iA}, \quad (2)$$

and this was carried out over a short period of time; the width of the time window was $\tau = 20$ ps and 50 ps for water and counterions, respectively. The data for $\mathrm{MSD}(t)$ for every time slice (representing a fixed location along the box z-axis) was averaged separately for water molecules and ions over the total simulation time of 150 ns. Finally, we computed the short-time diffusion factor M by following the Einstein relation for the self-diffusion coefficient [45] and using a linear fitting of $\mathrm{MSD}_A(t)$. The factor M is computed largely in a similar manner as the hydrodynamic diffusion coefficient, but now without the long-time limit. For the same reason, since M is not defined in the hydrodynamic long-time limit, we call it as a diffusion factor instead of the true diffusion coefficient.

3. Results

Three different simulation setups were prepared for $AuNP^-$: EC, EC with salt, and IC (Fig. 1 and Table 1). The distance between $AuNP^-$ and the COM of the closest membrane along the z-axis of the box (bilayer surface normal) is shown in Fig. 2. For comparison, the distance between the membrane COMs in the double bilayer system is approximately 15 nm (~11 nm with respect to the phosphate groups in the leaflets facing each other across the water phase). The radius of $AuNP^-$ is approximately 2 nm. The $AuNP^-$ membrane distance of ~5.5 nm corresponds to the situation where the nanoparticle is at the center of the simulation box between the membranes.

On the EC side, $AuNP^-$ approaches the extracellular leaflet within a few tens of nanoseconds in all five simulations regardless of the initial conditions (for atomic velocities) and with and without added salt, whereas in IC it stays in the middle of the compartment and does not approach the membranes during the time scale of the five separate simulations. Hence, it can be concluded that the nanoparticle attaches to the EC leaflet and thereby the functional groups of $AuNP^-$ and the zwitterionic surface groups of the EC leaflet are in close contact. Meanwhile, there is no contact between $AuNP^-$ and the IC leaflet during the course of the simulation.

Partial densities for groups of atoms were calculated after equilibration for a time window of 50–200 ns, using the trajectories of long simulations. Results are given along the vertical simulation box axis in Fig. 3. They show that here the nanoparticle binding in EC occurs on the opposite surfaces in systems with and without salt (Fig. 3a,b), which is not surprising considering the identical composition of the two membranes. The partial density overlap between $AuNP^-$ and the membranes demonstrate that when the nanoparticle is in the EC compartment, it is in a stable contact with the membrane, interacting with the choline head groups. Instead, when $AuNP^-$ resides in the IC compartment, the density profile shows a broader distribution for $AuNP^-$ around the

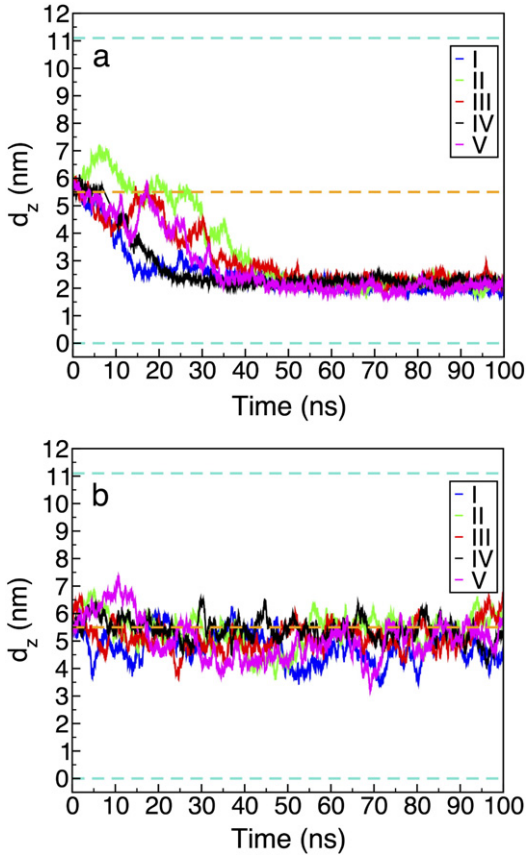

Fig. 2. Distance between $AuNP^-$ and membrane for five independent simulations. The distance is defined between $AuNP^-$ (metallic core COM) and the closest membrane surface, where the surface position is defined by its phosphate group COMs along the z-axis of the simulation box (bilayer surface normal). Data is given for both systems: $AuNP^-$ in (a) EC and (b) IC. The radius of $AuNP^-$ is approximately 2 nm, thus the AuNP-membrane surface distance of 2 nm corresponds to a situation where $AuNP^-$ has adsorbed to the bilayer surface. The turquoise and orange dashed lines present the approximative positions of the membrane surfaces and the simulation box center, respectively.

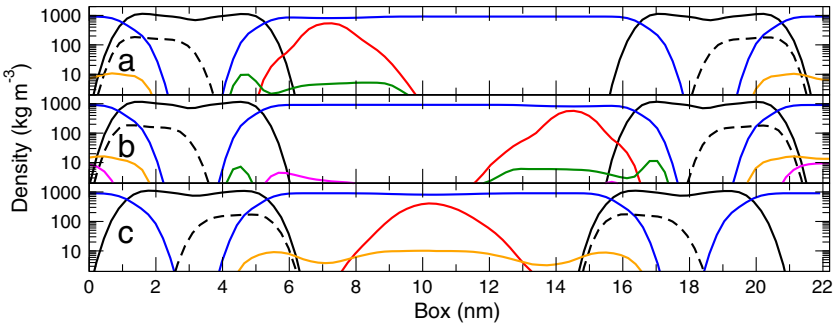

Fig. 3. Partial densities of $AuNP^-$ systems in (a) EC, (b) EC with salt, and (c) IC. Color code: membrane (black full line), NP (red full line), water (blue full line), POPS (black dashed), K^+ (orange full line), Cl^- (magenta full line), and Na^+ (green full line). In EC (a, b), the nanoparticle can attach to both membranes with equal probability.

compartment center (Fig. 3c), reflecting fluctuations of the nanoparticle position in bulk water phase. Clearly, there is no tendency for $AuNP^-$ to bind with the IC leaflet.

In EC, the ionic cloud of Na^+ around $AuNP^-$ is rather compact, but strongly biased towards the neighboring leaflet. The counterions have small maxima overlapping with the membrane due to contacts with (negative) phosphates. Interestingly, the EC system with salt (Fig. 3b) shows that Na^+ and Cl^- counterions have accumulated on the opposite membrane surface with respect to the nanoparticle; this is coupled to the attraction between POPC lipids and Na^+ and the high surface charge density of $AuNP^-$ repels Cl^-. The electrostatic interactions are mediated through the whole compartment (and beyond it), and the nanoparticle attachment is a co-operative process which involves all components in the solvent. Furthermore, the K^+ content on the IC side is already rather substantial without additional salt as the $AuNP^-$ and POPS counterions add up in a continuous distribution across the whole compartment, which screens the electrostatic interaction experienced by both the nanoparticle and the membrane surface (see Fig. 3c).

In order to get more insight on the role of counterions in the binding of the nanoparticle with a membrane, in Fig. 4 we consider the distribution of Na^+ (K^+) around $AuNP^-$ in the EC (IC) compartment, averaged over 60 ns simulations. Here, the nanoparticle COM has been constrained to a distance of 2.8 nm from the membrane, which is close to the average binding distance in the EC case. In the IC case, one has to bear in mind that the situation is only suggestive, since in our non-biased simulations we did not observe $AuNP^-$ to spontaneously attach to the IC leaflet (see Fig. 2), and when $AuNP^-$ was taken to the IC surface and released, it moved quite rapidly (within tens of nanoseconds) back to the water phase (data not shown). Nonetheless, in both cases the counterions form a halo-pattern around $AuNP^-$, and the ripples close to the terminal COO^- groups demonstrate equidistant positions for the terminal groups and the organized solvent structure (ionic contacts and hydrogen bonds of water). Both cases also highlight the strength of electrostatic interaction, resulting in considerable aggregation of cationic counterions with $AuNP^-$, and showing how the entropic contribution to drive counterions to the water phase is quite weak here.

On the IC side, the larger number of K^+ compared to the EC case is evident (Fig. 4), as there is a larger concentration of counterions between or close to $AuNP^-$ and the membrane. The system responds in this way to an energetically unfavorable situation where the positive counterion charge is balancing the negative charge of the nanoparticle and the negatively charged membrane surface. Unlike for the cationic Au nanoparticle and Cl^- [17,18], the cations are able to enter between the nanoparticle side chains, but the slightly positive effective charge of the metallic core hinders cations from penetrating deeper. One should also note that the POPS lipids are more exposed to the solvent (IC) due to the electrostatic interactions with K^+ ions.

The average number and the lifetime of H-bonds and ion contacts between $AuNP^-$ and solvent (Table 2) show small differences between the EC and IC solutions: The total number of H-bonds between $AuNP^-$ terminal carboxylate groups and water is reduced from 397.7 ± 1.6 to 371.1 ± 1.1 by a change from EC to IC (note that there are 60 side chains and two H-bond acceptor atoms per terminal carboxylate group), and the corresponding lifetimes decrease similarly from 4.7 ± 0.3 ps to 3.3 ± 0.1 ps. This difference in water coordination is coupled with the

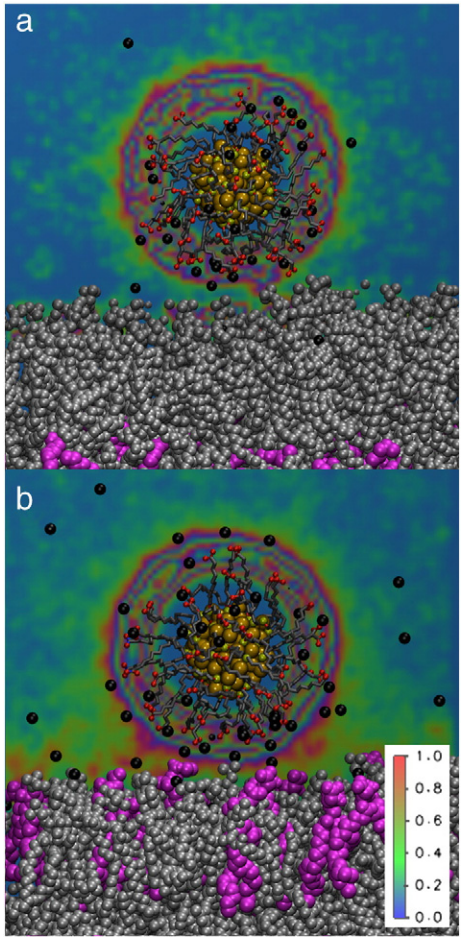

Fig. 4. Visualization of $AuNP^-$ with (a) Na^+ counterions in EC, and (b) K^+ counterions in IC cut-plane presentation, color code from high (max 1.0) to low (min 0.0) concentrations: purple, red, green, and blue. Elevated concentration of counterions (green color) around the nanoparticle is obvious. The distance between the nanoparticle center and the POPC head groups of the nearest leaflet has been fixed to 2.8 nm in both cases. The counterion concentrations are averaged over 60 ns simulations. Color code, molecules: Na^+/K^+ (black), and POPS lipids (magenta).

number of counterion contacts (see below, Na^+ in EC and K^+ in IC). The longer H-bond lifetime values for water in EC can be explained by the $AuNP^-$ membrane interactions: The movement of $AuNP^-$ is restricted in EC due to the membrane attachment, and this causes its water solvation shell to be less interrupted and consequently the H-bonds live longer. Furthermore, the water mobility itself is reduced close to the membrane surface (see below).

The number of ion contacts differs by an order of magnitude between EC and IC: 3.0 ± 0.3 for Na^+ in EC and 42.7 ± 1.2 for K^+ in IC. The difference is partially explained by the fact that there are K^+ counterions present for both POPS lipids and $AuNP^-$ in the IC compartment. The ion contact lifetimes in IC are twice the lifetimes in EC, which is presumably related to the number of counterions in the solution and the repulsive ion–ion interactions in the $AuNP^-$ surroundings.

The counterion concentration affects the H-bonds as well, and the number of H-bonds with water is smaller in IC than in EC as the numerous contacts with ions diminish the number of H-bonds between the $AuNP^-$ terminal groups and water. For EC, the number of Na^+ ion contacts and lifetimes is similar to those observed earlier [18] for the same $AuNP^-$ in an aqueous solution without the presence of bilayers, 4.4 ± 0.4 and 10.1 ± 1.1 ps. The same applies to H-bonds where the corresponding values were 404.4 ± 0.5 and 3.5 ± 0.1 ps in an aqueous environment. Adding salt to the EC system does not significantly affect the numbers of contacts or lifetimes between $AuNP^-$ and the solvent.

Table 2 also lists values for the contacts between $AuNP^-$ and membranes, and the results show similar trends for the EC compartment with and without salt. The nanoparticle-membrane contact lifetimes are <15 ps, which is rather short and indicates that $AuNP^-$ readily diffuses along the membrane surface. Small values for the membrane contacts indicate that $AuNP^-$ remains close to the surface of the EC leaflet, not penetrating deeply inside the membrane since it experiences the electrostatic repulsive force caused by the negatively charged lipid phosphate groups and the POPS lipids in the cytosolic leaflet. Concerning the number of water-membrane contacts, there are more of those in the IC compartment where $AuNP^-$ is not attached, as this leaves more lipid surface groups exposed to the water solvent (data not shown).

The nanoparticle–membrane interactions described above are to some extent reflected in the order parameters of lipids, too, shown in Fig. 5. In the EC compartment without added salt (Fig. 5a), the POPC order parameters are largely the same regardless of the present of $AuNP^-$. When salt is added, the order parameter increases about 5–10% compared to the reference system, but this is likely due to monovalent salt that is known to decrease the area per lipid in the membrane, thereby increasing membrane order, and stems from salt ion-induced lipid clustering[46–48].

Additional analysis of the nearby lipids within 3 nm from the $AuNP^-$ COM and without salt shows a slight reduction of the outermost carbon atom order parameters (increased disorder) due to the interaction with the terminal COO^- groups, but the effect is subtle. In the IC compartment without additional salt, the results shown in Fig. 5b indicate the ordering of POPCs to increase and the ordering of POPS lipids to decrease due to the presence of $AuNP^-$. It should be noted that $AuNP^-$ brings along 60 K^+ counterions which add up with the initial counterion balancing the POPS charge. It seems likely that the repulsive interactions between $AuNP^-$ and POPS give rise to lateral lipid reorganization where POPSs are displaced underneath $AuNP^-$, making room for a POPC-rich lipid region right under the nanoparticle. We consider that this phenomenon is possibly an artificial finite-size effect since $AuNP^-$ would drift farther from the IC surface in a larger simulation compartment.

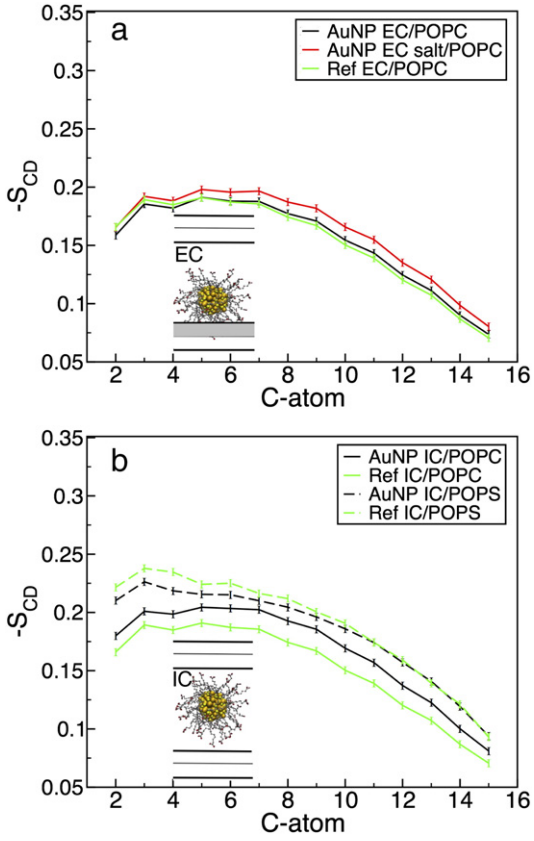

Fig. 5. Order parameter results for POPC lipids in the EC and IC leaflets, in the presence/absence of $AuNP^-$. (a) EC compartment, data in the leaflet that is the closest to $AuNP^-$. (b) IC compartment, where $AuNP^-$ is largely in the middle of the water phase, the results shown here are an average of the two IC leaflets. Color coding in both panels corresponds to the $AuNP^-$ system without added salt (black), the $AuNP^-$ system with added salt (red), and the reference system without $AuNP^-$ and without additional salt (green). The results were computed over a period of 150 ns, each, and for saturated carbon chains only. The error bars are ±0.001 based on the largest observed value.

Table 2
Hydrogen bonds and contacts between $AuNP^-$ and solvent/lipids. N_A is the average number of hydrogen bonds or contacts between $AuNP^-$ and a solvent molecule/lipid, A. τ_A is the average lifetime of the contacts.

Compartment	A	N_A	τ_A [ps]
EC	H_2O	397.7 ± 1.6	4.7 ± 0.3
	Na^+	3.0 ± 0.3	9.8 ± 0.5
	Lipid	5.0 ± 2.5	15.3 ± 2.2
EC with salt	H_2O	399.4 ± 0.7	4.2 ± 0.2
	Na^+	3.6 ± 0.4	10.3 ± 1.9
	Lipid	4.6 ± 0.5	15.3 ± 1.4
IC	H_2O	371.1 ± 1.1	3.3 ± 0.1
	K^+	42.7 ± 1.2	20.9 ± 0.2
	Lipid	–	–

The short-time diffusion factors of water molecules and counterions are shown in Fig. 6 (water) and Fig. 7 (counterions). They have been determined inside 0.5 nm and 1.0 nm thick lateral slices, respectively, along the membrane(s) surface normal in the $AuNP^-$ host compartment. In general, the water/counterion diffusion factors are reduced close to membrane surfaces. We remind that $AuNP^-$ attaches to the membrane surface in EC, but it stays at the middle of the compartment in IC. This behavior is evident in the distribution shapes as the water diffusion is reduced near $AuNP^-$, and the same effect is visible for the Na^+/K^+ counterions, too. Water forms an H-bond network around the terminal groups of $AuNP^-$ (and counterions), and this makes the H_2O positions more restricted close to the nanoparticle. For water, the change in diffusion as a function of distance is smaller than for counterions. This can be explained by the type of bonds/contacts that water and ions form with $AuNP^-$: H-bonds between the terminal COO^- groups and water are weaker and of shorter range than the electrostatic interactions with counterions. Finally, the nanoparticle attachment (EC) results in an increase in solvent mobility at the opposite membrane

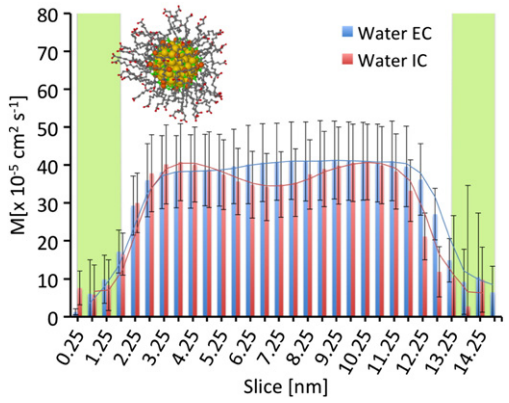

Fig. 6. Mobility of water between membranes. The short-time diffusion factor has been calculated for water molecules (with respect to oxygen) inside $\Delta r = 0.5$ nm thick slices along the z-axis of the simulation box (along the membrane surface normal) between the two membranes averaged over the 50–200 ns simulation time. The histograms in EC and IC are presented using blue and red colors, respectively. The error bars correspond to standard deviations. The zero-level has been defined with respect to the membrane center plane, and the green bars stand for the membrane surface planes.

surface, highlighting the fact that the $AuNP^-$ movement is reflected throughout the whole compartment, also in terms of dynamics.

As noted in previous work for cationic and anionic AuNPs in aqueous environment, [18] the choice of terminal groups (amine/carboxylate) affects the surrounding H-bond network, as evidenced for the H_2O orientations as a function of distance from the nanoparticle center. Similar plots are presented for $AuNP^-$ in the EC and IC compartments in Supplementary Fig. 1. As shown in Fig. 6, the effect of $AuNP^-$ on the diffusion of solvent extends rather far (several nanometers), implying that the solvent transmits the interaction shell-by-shell by intermediating the orientation of water molecules. This phenomenon is evident in the data for water orientations, which depend strongly on the distance: The first shell surrounding the COO^- terminal groups aligns water molecules in such a manner that hydrogens are pointing towards $AuNP^-$ (carboxylates). This effect arises from the electrostatic forces between the COO^- groups and polarized water molecules. The differences between the two compartments, EC and IC, are very small despite the fact that $AuNP^-$ is in contact with the membrane surface in EC.

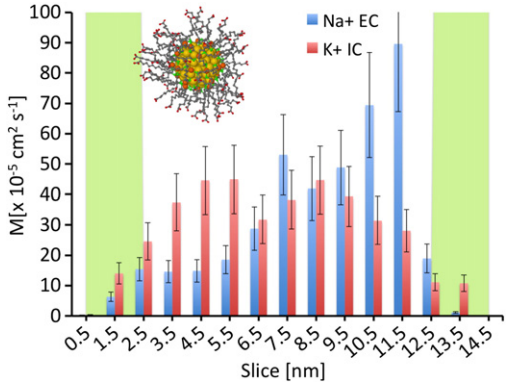

Fig. 7. Short-time diffusion factor (M) of counterions shown as a function of distance from one of the membrane leaflets facing the given compartment (EC or IC), and extending across the water phase to the surface of the other leaflet in the same compartment. The results have been averaged over a period of 50–200 ns after the 50 ns equilibration period. Results in the EC (IC) compartments are shown in blue (red) color. The error bars correspond to standard deviation. The zero-level has been defined with respect to the membrane center plane, and the green bars stand for the membrane surface planes.

4. Discussion and conclusions

Gold nanoparticles are being used extensively in biomedicine and nanotechnology, and assessing their potential health hazards is extremely timely. Here, revealing the atomistic details of their interactions with biomolecules and cell membranes is very relevant. To clarify the underlying molecular processes in such system, we have performed a series of MD simulations at atomistic scale for a monolayer-protected $AuNP^-$ with functionalized (negatively charged) alkanethiol side groups interacting with a realistic model lipid membrane system. The nanoparticle composition matches with one of the most ubiquitous synthesized AuNP sizes (29 kDa, 2 nm) and its mass-spectrometrical analysis ($Au_{144}(SR)_{60}$). Furthermore, the nanoparticle structure incorporates the recently found structural motifs of ligand-protected AuNPs where the metallic Au core is a nearly-spherical polyhedron, and part of Au atoms participate (in oxidized form) in the Au-SR ligand-shell.

Our model for the membrane is based on a double membrane setup able to describe the extracellular (EC) and intracellular (IC, cytosolic) compartments with different salt and counterion distributions, and the asymmetricity of lipid bilayers, thus mimicking the real animal plasma membranes. Given that our model systems also include an explicit solvent, it is fair to conclude that the present approach includes several very detailed features that have not been included in previous (simulation) studies [19–24], except for a recent work on cationic AuNPs [17]. However, it is impossible (as well as out of the scope of this work) to model the complexity of a real mammalian cell and the diversity of all of its components. Further developments of the model could include, *e.g.*, integral membrane proteins and essential lipid components (such as cholesterol and sphingomyelin).

Experimental results suggest that the nanoparticle–membrane interaction depends on the AuNP charge as well as the nature and arrangement of the protecting side groups. That is to say, it is not the Au core that determines the interaction with the membrane but the surfactant layer on top of it. While cationic nanoparticles are known to penetrate through the cell membrane, less activity has been observed for anionic AuNPs [16]. The anionic AuNPs used in the experiments of Tatur *et al.* [16] had mercaptoundecanoic acid ($-S(CH_2)_{10}COOH$) surface groups, which are similar to the ones used in this study (with a difference of one CH_2 unit). Another study on anionic AuNP permeation by Van Lehn *et al.* [15] used 11-mercaptoundecane sulfonate ($-S(CH_2)_{11}SO_3-$) and octanethiol ($-S(CH_2)_7CH_3$) ligands with varying morphologies. These surface groups differ from the ones presented here.

We observed for $AuNP^-$ that it attached spontaneously to the EC membrane surface within a few tens of nanoseconds. It seems evident that the binding of $AuNP^-$ with the membrane takes place through relatively weak contacts with the zwitterionic POPC head groups, since $AuNP^-$ did not immerse deeply in the membrane but floated on top of the bilayer surface, enabling lateral diffusion of the nanoparticle along the membrane. In the IC compartment, we found that $AuNP^-$ stayed in the middle of the compartment, with no adsorption to the membrane. Apparently there is no attractive interaction with the cytosolic leaflet due to the Coulomb repulsion between $AuNP^-$ and the negatively charged POPS lipids.

Based on the results, it seems that $AuNP^-$ has no tendency to cross the membrane or bind to its surface, either in EC or IC. However, if it would, it is not clear whether it would pass or remain in the middle of the membrane. After all, one possible scenario is that the charged side groups of $AuNP^-$ would be stabilized by the charged regions of the membrane lipids, while the core of the nanoparticle (with $(CH_2)_{11}$ chains) would reside in the hydrophobic membrane interior. This kind of NP-embedding involving lipid rearrangement has been observed, *e.g.*, for charged dendrimers [49].

One of the grand questions in the field concerns the influence of nanoparticles on the function of membrane-associated proteins [50–52]. While we cannot unlock this question through our work,

let us consider the key background factor related to this theme: the binding of nanoparticles to membranes. In a previous work [17], it was shown that while cationic $AuNP^+$ avoided adsorption to the EC leaflet due to electrostatics, the binding of $AuNP^+$ to the EC leaflet yet took place through the crossing of a free energy barrier (about 12 kJ/mol) that is quite comparable to thermal energy, suggesting that the rate of spontaneous $AuNP^+$ binding to the EC side would be quite reasonable. On the IC side, $AuNP^+$ was observed to adsorb to the membrane in no time due to strong electrostatic attraction with anionic POPS [17]. Here in this work, $AuNP^-$ was observed to bind to the membrane on the EC side, and this binding was driven by electrostatics. On the IC side, the anionic nanoparticle avoided contact with the membrane due to anionic POPS lipids. Moreover, $AuNP^-$ was observed to maximize its distance from the IC leaflet, suggesting that in the cytosol $AuNP^-$ would not favor being in any close proximity to the intracellular leaflet of the plasma membrane, assuming that there are no additional charged entities (fluctuations in lipid concentration, biomolecules).

Summarizing, these observations, comparisons, and earlier studies [5,15,17,23,53] highlight the importance of electrostatic interactions in the binding of nanoparticles with membrane surfaces. The research results suggest that once nanoparticles have attached to a membrane surface, they prefer to interact with membrane proteins whose juxtamembrane domains are appropriately charged or polar, or with proteins whose ectodomains (in the extracellular space) or cytosolic domains favor interactions with the given nanoparticle. Both situations are problematic considering protein function as they can potentially change protein conformation. As a single example, one of the key processes in cell membranes is communication driven by membrane receptors binding with their extracellular ligands. If the conformation of the receptor was altered by a strong interaction with a nanoparticle that is attached to the membrane, its visibility could be impaired, thus slowing down the signaling process, and this can be expected to influence cellular function. Detailed simulation studies testing this potential scenario would be welcome. In the meantime, this scenario is supported by the observation that $AuNP^+$ binds to plasma membrane-like lipid bilayers more efficiently than $AuNP^-$, in agreement with experiments that have shown cationic gold nanoparticles to be more harmful to model membranes than anionic ones [16].

Even though there exists a large body of literature published on the research of nanomaterials, the field still lacks systematic mapping of all the factors that are (or potentially might be) involved in the interactions between various kinds of studied nanoparticles and cells. Hence, it is of importance to perform detailed studies of specific model systems to clarify the effects of individual variables. For achieving a conclusive perspective, it is necessary to complement the computational results by experiments, and *vice versa*. The *in silico* predictions presented here could quite straightforwardly be verified experimentally using simplified POPC/POPS model membranes with corresponding $AuNP^-$, *i.e.*, in similar manner as in the recent study of Tatur *et al.* [16].

Concluding, the results presented in this study bring more weight to the idea that electrostatic interactions are particularly important in the nanoparticle-membrane binding, and that these may have consequences for cellular function.

Acknowledgement

The computations were performed on the Juropa (Intel Xeon 5570) and Cray XT4/XT5 computers in the Forschungszentrum Jülich (Germany) and CSC — IT Centre for Science Ltd (Espoo, Finland). Financial support has been provided by the Academy of Finland through its Centre of Excellence Programs (project 251748 for EH and JA; project 272130 for HMS and IV). IV also acknowledges support from the European Research Council (advanced grant CROWDED-PRO-LIPIDS).

Appendix A. Supplementary data

Supporting information contains additional data for the orientation of water molecules around $AuNP^-$, the radial distribution functions centered at $AuNP^-$, and the radius of gyration and the moment of inertia vector autocorrelation function of $AuNP^-$ in the EC and IC compartments. Supplementary data to this article can be found online at http://dx.doi.org/10.1016/j.bbamem.2014.07.027.

References

[1] E.C. Dreaden, A.M. Alkilany, X. Huang, C.J. Murphy, M.A. El-Sayed, The golden age: gold nanoparticles for biomedicine, Chem. Soc. Rev. 41 (2012) 2740–2779.
[2] L. Dykman, N. Khlebtsov, Gold nanoparticles in biomedical applications: recent advances and perspectives, Chem. Soc. Rev. 41 (2012) 2256–2282.
[3] A. Nel, T. Xia, L. Mädler, L. Ning, Toxic potential of materials at the nanolevel, Science (2006) 622–627.
[4] N. Khlebtsov, L. Dykman, Biodistribution and toxicity of engineered gold nanoparticles: a review of in vitro and in vivo studies, Chem. Soc. Rev. 40 (2011) 1647–1671.
[5] C.M. Goodman, C.D. McCusker, T. Yilmaz, V.M. Rotello, Toxicity of gold nanoparticles functionalized with cationic and anionic side chains, Bioconjug. Chem. 15 (2004) 897–900.
[6] R.A. Sperling, P.R. Gil, F. Zhang, M. Zanella, W.J. Parak, Biological applications of gold nanoparticles, Chem. Soc. Rev. 37 (2008) 1896–1908.
[7] N. Lewinski, V. Colvin, R. Drezek, Cytotoxicity of nanoparticles, Small 4 (2008) 26–49.
[8] A.M. Alkilany, P.K. Nagaria, C.R. Hexel, T.J. Shaw, C.J. Murphy, M.D. Wyatt, Cellular uptake and cytotoxicity of gold nanorods: molecular origin of cytotoxicity and surface effects, Small 5 (2009) 701–708.
[9] C.J. Murphy, M.G. Anand, J.W. Stone, P.N. Sisco, A.M. Alkinaly, E.C. Goldsmith, S.C. Baxter, Gold nanoparticles in biology: beyond toxicity to cellular imaging, Acc. Chem. Res. 41 (2008) 1721–1730.
[10] Y. Pan, A. Leifert, D. Ruau, S. Neuss, J. Bornemann, G. Schmid, W. Brandau, U. Simon, W. Jahnen-Dechent, Gold nanoparticles of diameter 1.4 nm trigger necrosis by oxidative stress and mitochondrial damage, Small 5 (2009) 2067–2076.
[11] A. Verma, O. Uzun, Y. Hu, Y. Hu, H.-S. Han, N. Watson, S. Chen, D.J. Irvine, F. Stellacci, Surface-structure-regulated cell-membrane penetration by monolayer-protected nanoparticles, Nat. Mater. 7 (2008) 588–595.
[12] A. Mecke, D.-K. Lee, A. Ramamoorthy, B.G. Orr, M.M. Banaszak Holl, Synthetic and natural polycationic polymer nanoparticles interact selectively with fluid-phase domains of DMPC lipid bilayers, Langmuir 21 (2005) 8588–8590.
[13] P.R. Leroueil, S.A. Berry, K. Duthie, G. Han, V.M. Rotello, D.Q. McNerny, J.R. Baker Jr., B. G. Orr, M.M. Banaszak Holl, Wide varieties of cationic nanoparticles induce defects in supported lipid bilayers, Nano Lett. 8 (2008) 420–424.
[14] J. Chen, J.A. Hessler, K. Putchakayala, B.K. Panama, D.P. Khan, S. Hong, D.G. Mullen, S.C. DiMaggio, A. Som, G.N. Tew, A.N. Lopatin, J.R. Baker, M.M. Banaszak Holl, B.G. Orr, Cationic nanoparticles induce nanoscale disruption in living cell plasma membranes, J. Phys. Chem. B 113 (2009) 11179–11185.
[15] R. Van Lehn, P.U. Atukorale, R.P. Carney, Y.-S. Yang, F. Stellacci, D.J. Irvine, A. Alexander-Katz, Effect of particle diameter and surface composition on the spontaneous fusion of monolayer-protected gold nanoparticles with lipid bilayers, Nano Lett. 13 (2013) 4060–4067.
[16] S. Tatur, M. Maccarini, R. Barker, A. Nelson, G. Fragneto, Effect of functionalized gold nanoparticles on floating lipid bilayers, Langmuir 29 (2013) 6606–6614.
[17] E. Heikkilä, H. Martinez-Seara, A. Gurtovenko, I., V., H. Häkkinen, J. Akola, Cationic Au nanoparticle binding with plasma membrane-like lipid bilayers: potential mechanism for spontaneous permeation to cells revealed by atomistic simulations, J. Phys. Chem. 118 (2014) 11131–11141.
[18] E. Heikkilä, A. Gurtovenko, H. Martinez-Seara, I. Vattulainen, H. Häkkinen, J. Akola, Atomistic simulations of functional $Au_{144}(SR)_{60}$ gold nanoparticles in aqueous environment, J. Phys. Chem. C 116 (2012) 9805–9815.
[19] Y. Li, X. Chen, N. Gu, Computational investigation of interaction between nanoparticles and membranes: hydrophobic/hydrophilic effect, J. Phys. Chem. B 112 (2008) 16647–16653.
[20] Y. Li, N. Gu, Thermodynamics of charged nanoparticle adsorption on charge-neutral membranes: a simulation study, J. Phys. Chem. B 114 (2010) 2749–2754.
[21] J. Lin, H. Zhang, Z. Chen, Y. Zheng, Penetration of lipid membranes by gold nanoparticles: insights into cellular uptake, cytotoxicity, and their relationship, ACS Nano 4 (2010) 5421–5429.
[22] Y. Li, X. Li, Z. Li, H. Gao, Surface-structure-regulated penetration of nanoparticles across a cell membrane, Nanoscale 4 (2012) 3768–3775.
[23] R.C. Van Lehn, A. Alexander-Katz, Free energy change for insertion of charged, monolayer-protected nanoparticles into lipid bilayers, Soft Matter 10 (2014) 648–658.
[24] J. Lin, A. Alexander-Katz, Cell membranes open "Doors" for cationic nanoparticles/biomolecules: insights into uptake kinetics, ACS Nano 7 (2013) 10799–10808.
[25] Y. Li, Z. Yang, N. Hu, R. Zhou, X. Chen, Insights into hydrogen bond dynamics at the interface of the charged monolayer-protected Au nanoparticle from molecular dynamics simulation, J. Chem. Phys. 138 (2013) (184703–1–9).
[26] R.C. Van Lehn, A. Alexander-Katz, Structure of mixed-monolayer-protected nanoparticles in aqueous salt solution from atomistic molecular dynamics simulations, J. Phys. Chem. C 117 (2013) 20104–20115.

[27] H.J.C. Berendsen, D. van der Spoel, R. van Drunen, GROMACS: a message-passing parallel molecular dynamics implementation, Comp. Physiol. Commun. 91 (1–3) (1995) 43–56.
[28] O. Lopez-Acevedo, J. Akola, R. Whetten, H. Grönbeck, H. Häkkinen, Structure and bonding in the ubiquitous icosahedral metallic gold cluster $Au_{144}(SR)_{60}$, J. Phys. Chem. C 113 (2009) 5035–5038.
[29] L.L.M. Van Deenen, J.A.F.O. den Kamp, B. Roelofsen, K.W.A. Wirtz, On membrane phospholipids and protein-lipid association, Pure Appl. Chem. 54 (1982) 2443–2454.
[30] A.A. Spector, M.A. Yorek, Membrane lipid composition and cellular function, J. Lipid Res. 26 (1985) 1015–1103.
[31] A.A. Gurtovenko, I. Vattulainen, Membrane potential and electrostatics of phospholipid bilayers with asymmetric transmembrane distribution of anionic lipids, J. Phys. Chem. B 112 (2008) 4629–4634.
[32] O. Berger, O. Edholm, F. Jähnig, Molecular dynamics simulations of a fluid bilayer of dipalmitoylphosphatidylcholine at full hydration, constant pressure, and constant temperature, Biophys. J. 72 (1997) 2002–2013.
[33] D.P. Tieleman, H.J.C. Berendsen, A molecular dynamics study of the pores formed by *Escherichia Coli* OmpF porin in a fully hydrated palmitoyloleoylphosphatidylcholine bilayer, Biophys. J. 74 (1998) 2786–2801.
[34] M. Bachar, P. Brunelle, D.P. Tieleman, A. Rauk, Molecular dynamics simulation of a polyunsaturated lipid bilayer susceptible to lipid peroxidation, J. Phys. Chem. B 108 (2004) 7170–7179.
[35] P. Mukhopadhyay, L. Monticelli, D.P. Tieleman, Molecular dynamics simulation of a palmitoyl–oleoyl phosphatidylserine bilayer with Na + counterions and NaCl, Biophys. J. 86 (2004) 1601–1609.
[36] H.J.C. Berendsen, J.P.M. Postma, W.F. van Gunsteren, J. Hermans, Intermolecular Forces, in: B. Pullman (Ed.), Reidel, Dordrecht, 1981, (Chapter Interaction models for Water in Relation to Protein Hydration).
[37] D.P. Tieleman, H.J.C. Berendsen, Molecular dynamics simulations of a fully hydrated dipalmitoylphosphatidylcholine bilayer with different macroscopic boundary conditions and parameters, J. Chem. Phys. 105 (1996) 4871–4880.
[38] U.L. Essmann, L. Perera, M.L. Berkowitz, T. Darden, H. Lee, L.G.A. Pedersen, Smooth particle mesh Ewald method, J. Chem. Phys. 103 (1995) 8577–8593.
[39] D. Van Der Spoel, E. Lindahl, B. Hess, G. Groenhof, A.E. Mark, H.J.C. Berendsen, GROMACS: fast, flexible and free, J. Comput. Chem. 26 (2005) 1701–1718.
[40] H.J.C. Berendsen, J.P.M. Postma, W.F. Van Gunsteren, A. Dinola, J.R. Haak, Molecular dynamics with coupling to an external bath, J. Chem. Phys. 81 (1984) 3684–3690.
[41] J.-P. Ryckaert, G. Ciccotti, H.J.C. Berendsen, Numerical integration of the Cartesian equations of motion of a system with constraints: molecular dynamics of *n*-alkanes, J. Comp. Physiol. 23 (3) (1977) 327–341.
[42] W. Humphrey, A. Dalke, K. Schulten, VMD — visual molecular dynamics, Mol. Graph. 14 (1) (1996) 33–38.
[43] GROMACS, User Manual Version 4.0, 2010.
[44] P. Chau, A.J. Hardwick, A new order parameter for tetrahedral configurations, Mol. Phys. 93 (1998) 511–518.
[45] P. Chaikin, T. Lubensky, Principles of Condensed Matter Physics, Cambridge University Press, Cambridge, 1995.
[46] R.A. Böckmann, A. Hac, T. Heimburg, H. Grubmüller, Effect of sodium chloride on a lipid bilayer, Biophys. J. 85 (2003) 1647–1655.
[47] A.A. Gurtovenko, I. Vattulainen, Effect of NaCl and KCl on phosphatidylcholine and phosphatidylethanolamine lipid membranes: insight from atomic-scale simulations for understanding salt-induced effects in the plasma membrane, J. Phys. Chem. B 112 (2008) 1953–1962.
[48] A. Cordomi, O. Edholm, J.J. Perez, Effect of force field parameters on sodium and potassium ion binding to dipalmitoyl phosphatidylcholine bilayers, J. Chem. Theory Comput. 5 (2009) 2125–2134.
[49] A.A. Gurtovenko, J. Anwar, I. Vattulainen, Defect-mediated trafficking across cell membranes: insights from in silico modelling, Chem. Rev. 110 (2010) 6077–6103.
[50] Z.J. Deng, M. Liang, M. Monteiro, I. Toth, R.F. Minchin, Nanoparticle-induced unfolding of fibrinogen promotes Mac-1 receptor activation and inflammation, Nat. Nanotechnol. 6 (2011) 39–44.
[51] H.L. Karlsson, P. Cronholm, Y. Hedberg, M. Tornberg, L. De Battice, S. Svedhem, I.O. Wallinder, Cell membrane damage and protein interaction induced by copper containing nanoparticles — importance of the metal release process, Nanotoxicology 313 (1) (2013) 59–69.
[52] M. Rahman, S. Laurent, N. Tawil, L. Yahia, M. Mahmoudi, Protein-Nanoparticle Interactions: The Bio-Nano Interface, Springer-Verlag, Berlin Heidelberg, 2013.
[53] L. Dykman, N. Khlebtsov, Uptake of engineered gold nanoparticles into mammalian cells, Chem. Rev. 114 (2014) 1258–1288.